Astron. Astrophys. 272, 621–633 (1993)

ASTRONOMY AND ASTROPHYSICS

A theoretical model for tilts of bipolar magnetic regions

S. D'Silva and A.R. Choudhuri

Department of Physics, Indian Institute of Science, Bangalore 560 012, India

Received June 1, accepted November 8, 1992

Abstract. Joy's law (Hale et al. 1919) states that bipolar magnetic regions (BMRs) are inclined to the latitudinal line, with the p-spot (preceding spot) of the BMR closer to the equator and the tilt angle increasing with latitude. It is believed that the solar dynamo operates in the overshoot region just below the convection zone and the BMRs are produced by the flux loops rising from there due to magnetic buoyancy. These rising loops are expected to be twisted by the Coriolis force so that they eventually emerge on the solar surface with a tilt. We extend the numerical calculations of Choudhuri (1989) to study the tilts produced on the rising flux loops by the Coriolis force. We find that the theoretically calculated tilts match the observations only if the magnetic field of the flux loops lies in the range between 60 and 160 kG. For such flux loops, the tilt has the correct magnitude and also varies correctly with the latitude. If the magnetic fields were stronger than 160 kG, then Coriolis force is much weaker than magnetic buoyancy and is only able to produce tilts which are very small in overall magnitude, though they still vary correctly with latitude. On the other hand, if the fields were smaller than 60 kG, then the Coriolis force would have been so overpowering that the flux loops would move parallel to the rotation axis as found earlier (Choudhuri 1989). Such flux loops appear only in high latitudes and do not obey Joy's law. On changing the drag on the flux tube, these conclusions are not changed. If we change the footpoint separation of the flux loop, then we find that magnetic tension may halt the rise of the flux loop if the footpoint separation is below a critical value. However, for flux tubes which are able to reach the surface, the range from 60 to 160 kG for the magnetic field still approximately holds. Thus our calculations seem to rule out either equipartition fields (about 10 kG) or very strong megagauss fields.

Key words: Sun: magnetic fields – sunspots – rotation, hydromagnetics

Send offprint requests to: A.R. Choudhuri

1. Introduction

In a classic paper by Hale et al. (1919), it was shown that the line joining the two poles of a bipolar region is always inclined at an angle to the E–W line, with the preceding spot (p-spot) closer to the equator and the following spot (f-spot) away from the equator. This angle, called the tilt, was found to vary linearly from 3° at the equator to 11° at 30° N or S latitude. This latitudinal dependence of the tilt, often called "Joy's Law", is confirmed by recent studies (Wang & Sheeley 1989, 1991; Howard 1992) and a least-square fit to the data has been given by Wang & Sheeley (1991) in the form $\sin(\text{tilt}) = 0.48 \sin(\text{latitude}) + 0.03$.

It is believed that the magnetic fields are generated by the dynamo operating in a stable layer at the base of the convection zone (see Choudhuri 1990a and references therein). Strands of magnetic flux, which may come out of this stable layer, would rise through the convection zone to produce the bipolar magnetic regions (BMRs) on the surface. Schmidt (1968) suggested that the Coriolis force twists the ascending flux loops and is responsible for the tilt of the BMRs. The aim of the present paper is to develop a detailed theoretical model to explain the tilts of the BMRs and to study whether the observed tilts can be used to impose constraints on the parameters pertaining to subsurface magnetic fields.

There remains a possibility that the tilts of BMRs can arise another way. All dynamo models (Parker 1955; Babcock 1961; Leighton 1964, 1969) suggest that a poloidal field is wound up by differential rotation to produce a toroidal field, which then erupts to form the familiar BMRs. The tilts of the BMRs could just be the pitch angle of the subsurface field. The main objection to this picture is that the tilts at a particular latitude should then decrease as the field lines are stretched further with the progress of the solar cycle. Such time dependence of tilt has not been observed (Wang & Sheeley 1989). Moreover, if the tilts reflect the pitch of the subsurface fields as shown in Fig. 1, then at any given time the tilts of the BMRs erupting at lower latitudes should show a larger tilt than those at

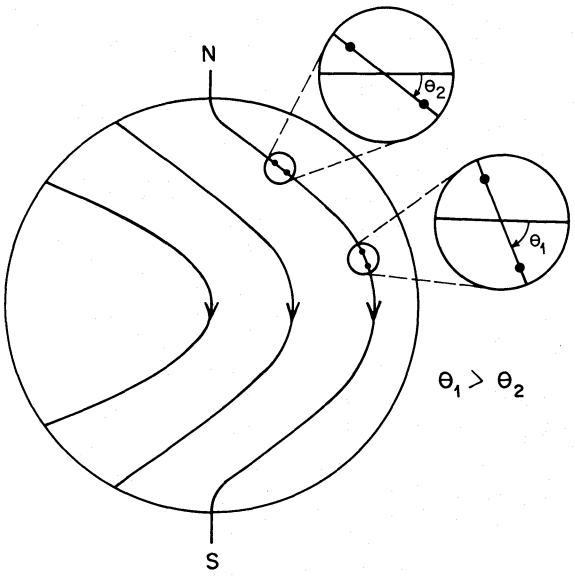

Fig. 1. Cartoon picture of the poloidal field being wound up to form the toroidal field. Tilts at lower latitudes θ_1 are greater than tilts at higher latitudes θ_2 if the BMRs reflect the pitch angle of the subsurface fields

higher latitudes. Because of these objections, twisting due to the Coriolis force provides a more satisfactory explanation for the tilts of BMRs.

The effect of the Coriolis force on rising flux tubes has been studied in a series of papers by Choudhuri and coworkers. Unless the magnetic field had a large value of about 100 kG or above, the Coriolis force was found to make the flux tubes move parallel to the rotation axis so that they eventually emerged at latitudes far poleward of the typical sunspot latitudes (Choudhuri & Gilman 1987; Choudhuri 1989). Only if the magnetic flux rises in the form of sufficiently thin tubes (a few hundred kilometers radius or so), then it was later found out that even weak magnetic fields can be made to come out radially by suppressing the Coriolis force with such special mechanisms as the rapid turbulent diffusion of angular momentum (Choudhuri & D'Silva 1990) or Kelvin–Helmholtz instability induced by the drag of giant cells (D'Silva & Choudhuri 1991). All these previous papers were mainly concerned with the question whether the flux tubes could be made to appear at the appropriate sunspot latitudes. We now study if the flux tubes appearing at the sunspot latitudes have the correct tilts. This is a non-axisymmetric problem which is handled by extending the non-axisymmetric code of Choudhuri (1989; hereafter Paper I).

It is impossible to say anything definite about the value of the magnetic field at the base of the convection zone from where it presumably starts rising. If the field is produced by the dynamo, one may naively expect the value to be equal to the equipartition value, which is probably not more than 10 kG (Parker 1987). Such weak fields are bound to be very much influenced by the Coriolis force. However, our understanding of the solar dynamo is still so primitive (see Choudhuri 1990a) that we should not probably take it for granted that the magnetic field has the equipartition value. Some authors have argued in favour of much stronger magnetic fields at the base of the convection zone (Moreno-Insertis et al. 1992). In fact, there are claims on the basis of helioseismology data that the field there may be as strong as a megagauss (Dziembowski & Goode 1989). In this paper, we take the point of view of not imposing any a priori restriction on the magnetic field. We study flux tubes with different initial magnetic fields and find that the observations of tilts allow the value of the magnetic field to lie only within a certain range.

We first calculate the tilts without incorporating any drag and using one flux loop in each quadrant. It is found that flux tubes having initial magnetic fields in the range from 60 to 160 kG come out radially with tilts close to the observed values. These are flux tubes for which the magnetic buoyancy is just able to overcome the Coriolis force, the rise time being comparable to the rotation period of the Sun. If the magnetic field were stronger, then the magnetic buoyancy would be so overpowering that the flux tube will come to the surface with negligible tilt. On the other hand, the weaker fields emerge at higher latitudes with tilts not consistent with observations. On incorporating the drag force and increasing the number of flux loops (which is equivalent to increasing magnetic tension), the results are not changed qualitatively. In this paper, we have not incorporated any of the special effects which are seen in the axisymmetric calculations to suppress the Coriolis force in the case of weak fields. Another paper (D'Silva 1993) will look at the question of whether weak fields (equipartition value or so) could be made to come out radially with correct tilts by invoking different special effects. When these various special effects are introduced, the parameter space of the problem becomes so large that it becomes impossible to draw clear conclusions. For the much cleaner problem of flux tubes with strong magnetic fields, we are able to draw one strong conclusion in this paper. The initial fields inside flux tubes could not be stronger than 160 kG. Otherwise we would not have seen any tilts at all in the bipolar regions.

All these calculations consider the convection zone to be a passive region with solid body rotation. Helioseismology observations (Dziembowski et al. 1989) show the evidence of differential rotation with contours of constant Ω lying roughly on cones. In the appendix we shall show that incorporating differential rotation does not affect the dynamics significantly.

We have used the thin flux tube equation of Spruit (1981), which was also used in the previous 2-dimensional simulations on the rise of flux tubes without incorporating the Coriolis force (Moreno-Insertis 1986; Chou & Fisher 1989). The thin flux tube equation breaks down when the flux tube reaches the topmost layers of the convection

zone, where the magnetic field inside the tube falls to very low values unless enhanced by surface effects not included here. The implict assumption throughout this paper is that the tilts are an eventual outcome of the increasng twists produced by the Coriolis force on flux tubes as they rise through the inner layers of the convection zone. The photospheric emergence, which cannot be handled by our code, has recently been studied by Shibata et al. (1989, 1990) through a 2-dimensional full MHD simulation.

Section 2 presents estimates of the tilt on the basis of a back-of-the-envelope calculation, which gives considerable insight with very little effort. After discussing the basic equations in Sect. 3, we describe in Sect. 4 how the tilt is estimated from a solution. Then Sect. 5 presents the results without drag for one flux loop in each quadrant. The next two sections respectively discuss how the results change with drag and magnetic tension. In Sect. 8, the final conclusions are summarized.

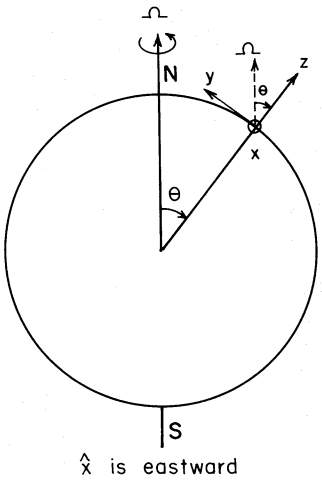

Fig. 3. Plot of the geometry considered for the rough calculations. The $\hat{z}$ direction is radially outward at the point O on the surface of the sphere, $\hat{x}$ is eastwards and $\hat{y}$ is northwards

2. Rough calculations

When a flux tube comes out of the stable dynamo layer, it rises to the surface due to magnetic buoyancy. If the two extreme ends of the flux tube remain anchored, then the tube takes the form of a loop. Magnetic buoyancy stretches this flux loop and makes the top of the loop emerge to the surface. The stretching of the loop makes particles in the tube move away from each other towards the two limbs of the loop as shown in Fig. 2. The Coriolis force acting on these particles moving away from each other is responsible for the tilting of the flux loop. It is mainly the stretching at the upper portion of the loop which causes the tilt. If a flux loop emerges radially (emerges at the same latitude at which it was formed) from the bottom of the convection zone, the stretching of the loop is equivalent to particles moving away from each other in the positive and negative ϕ-directions from the topmost point on the loop. The tilt caused by this stretching can be estimated by calculating the deflection of a particle in the positive x-direction in a local Cartesian system as shown in Fig. 3. The origin O is at the point where the top of the flux loop emerges from the surface, at a co-latitude of θ_{em}. The x-axis is along the East, z-axis is along the radius and y-axis is towards the North. Though the upper part of the loop rises as a whole, this motion does not contribute to the tilt, and one can get a fairly good estimate of tilt by considering only the relative motion between the topmost point and the nearby points moving away. The equation of motion for a particle traveling in the x-direction starting from (x_0, y_0, z_0) with an initial velocity $\boldsymbol{v}_0 = (v_{x,0}, 0, 0)$ can be written as

$$\frac{d\boldsymbol{v}}{dt} = 2\Omega[v_y \cos\theta_{em} - v_z \sin\theta_{em}]\hat{x} - 2v_x\Omega \cos\theta_{em}\hat{y} + 2v_x\Omega \sin\theta_{em}\hat{z}, \quad (1)$$

where $\Omega = 2.8\,10^{-6}\,s^{-1}$ is the rotational frequency of the Sun. The solution of Eq. (1) can be easily shown to be

$$x = x_0 + \frac{v_{x,0}}{2\Omega} \sin 2\Omega t, \quad (2a)$$

$$y = y_0 - \frac{v_{x,0}}{2\Omega}(1 - \cos 2\Omega t)\cos\theta_{em}, \quad (2b)$$

$$z = z_0 + \frac{v_{x,0}}{2\Omega}(1 - \cos 2\Omega t)\sin\theta_{em}. \quad (2c)$$

If γ is the deflection of the particle from the x-axis, then $\tan\gamma = \delta y/\delta x = (y - y_0)/(x - x_0)$, and γ is given as

$$\gamma = -\tan^{-1}(\tan\Omega t \cos\theta_{em}). \quad (3)$$

Equation (3) describes Joy's law. The negative sign indicates that the deflection is towards the equator, hence the p-spot is closer to the equator. It is independent of the initial velocity. For a particle traveling in the negative x-direction with an initial velocity $\boldsymbol{v}_0 = (-v_{x,0}, 0, 0)$, γ remains the same, indicating that the deflection is away from

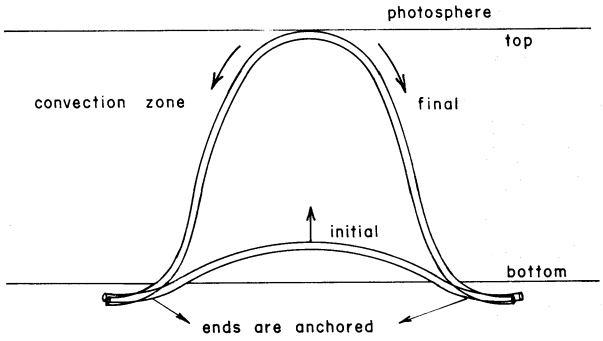

Fig. 2. Cartoon picture of the initial and the final configurations of a flux loop in the ξ–ϕ plane indicating the directions of magnetic buoyancy force and the mass downflows

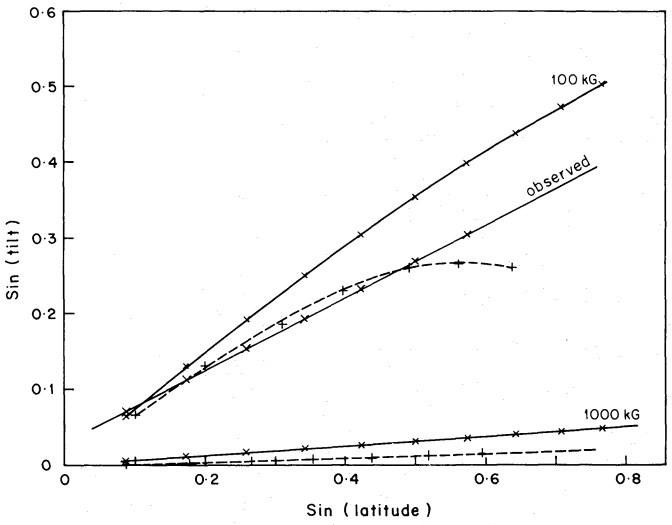

Fig. 4. Plot of sin (tilt) of BMRs emerging at different latitudes with sin (latitude) . Solid lines indicate the values of the rough calculations and dashed lines indicate the numerical calculations for 100 and 1000 kG fields as indicated

the equator, hence the f-spot is away from the equator. The factor $\cos\theta$ is responsible for the observed increase of tilt with increasing latitude. The proportionality of $\tan\gamma$ to $\cos\theta$ will henceforth be called the $\cos\theta$-effect.

The solution in Eq. (2c) also shows an asymmetric mass downflow. Particles moving in the direction opposite to the rotation (in the negative x-direction) move inwards (in the negative z-direction), whereas those moving along the rotation move outwards. This indicates that there is more mass downflow in the limb of the flux loop that gives rise to the f-spot. The numerical results indicate the same (Fig. 5c).

The value of tilt can be estimated by calculating the "rise time" – the amount of time required for a flux tube to traverse the convection zone. If the footpoint separation of the flux loop is large enough, magnetic tension becomes unimportant and the flux loop can be taken to be a flux tube which floats up to the surface from the bottom of the convection zone due to magnetic buoyancy. If the drag on the flux tube is the drag experienced by a cylinder moving perpendicular to its axis in a fluid, then the flux tube will attain a terminal velocity $v=(\pi\sigma/C_D H)^{1/2}v_A$ (Parker 1975), where σ is the radius of the flux tube, C_D is roughly a constant at very high Reynolds numbers and has a value of 0.4 (Goldstein 1938), H is the scale height and $v_A=B/\sqrt{4\pi\rho}$ is the Alfvén velocity inside the flux tube. The rise time may be taken to be $t=R_\odot/(3v)$, since the depth of the convection zone is about $R_\odot/3$. Taking $H\sim 6\,10^4$ km at the bottom of the convection zone and $\sigma\sim 1.5\,10^4$ km, we have $v\sim v_A$. The plots of $\sin\gamma$ with $\sin\lambda$ (λ is the latitude) for this case with magnetic fields $B=100$ and 1000 kG are given in Fig. 4. The agreement between the rough calculations (solid lines) and the numerical study (dashed lines) is striking. The numerical calculations are described in Sect. 5 and the values are taken from Fig. 6b. It is seen that a value of about 100 kG for the flux tube field makes the rough estimation comparable with observations.

Substituting the expression for the rise time in Eq. (1) we get

$$\gamma=-\tan^{-1}\left[\tan\left(\frac{\Omega R_\odot}{3}\sqrt{\frac{C_D H}{\pi}}\frac{1}{v_A\sqrt{\sigma}}\right)\cos\theta_{em}\right]. \qquad (4)$$

Clearly γ increases with decrease in magnetic field strength and flux tube size. Decreasing the flux tube size increases the drag on the flux tube and hence increases the rise time. Another factor that has been ignored till now is the magnetic tension. As we decrease the footpoint separation, the magnetic tension becomes important and the rise time increases due to the resistance to the motion offered by magnetic tension. Hence, the tilt should increase with decreasing footpoint separation. We shall see later that increasing drag and tension no doubt increases the tilt, but when they are made too large they inhibit the twisting of the flux loop. Thus increasing drag and tension does not increase the tilt indefinitely.

3. Mathematical equations

We carry out our calculations using the dynamical equation of a thin flux tube (Spruit 1981). The basic equation for a non-axisymmetric ring using spherical coordinates was discussed in Paper I. Here we reproduce the equations with an additional drag term:

$$\ddot{\xi}_n-\xi_n\dot{\theta}_n^2-\xi_n\dot{\phi}_n^2\sin^2\theta_n-2\omega\xi_n\dot{\phi}_n\sin^2\theta_n = \frac{M_n}{\xi_n^2}+L_n\frac{\xi_{n+1}-\xi_{n-1}}{|\xi_{n+1}-\xi_{n-1}|}+c_n(k'_n)_\xi+\frac{D_\xi}{\pi\sigma^2\rho_e(\xi_n)}, \qquad (5)$$

$$\xi_n\ddot{\theta}_n+2\dot{\xi}_n\dot{\theta}_n-\xi_n\dot{\phi}_n^2\sin\theta_n\cos\theta_n-2\omega\xi_n\dot{\phi}_n\sin\theta_n\cos\theta_n = L_n\frac{\xi_n(\theta_{n+1}-\theta_{n-1})}{|\xi_{n+1}-\xi_{n-1}|}+c_n(k'_n)_\theta+\frac{D_\theta}{\pi\sigma^2\rho_e(\xi_n)}, \qquad (6)$$

$$\xi_n\ddot{\phi}_n\sin\theta_n+2\dot{\xi}_n\dot{\phi}_n\sin\theta_n+2\xi_n\dot{\theta}_n\dot{\phi}_n\cos\theta_n+2\omega(\xi_n\dot{\theta}_n\cos\theta_n+\dot{\xi}_n\sin\theta_n) = L_n\frac{\xi_n\sin\theta_n(\phi_{n+1}-\phi_{n-1})}{|\xi_{n+1}-\xi_{n-1}|}+c_n(k'_n)_\phi+\frac{D_\phi}{\pi\sigma^2\rho_e(\xi_n)}, \qquad (7)$$

where $\xi_n=r_n/R_\odot$ and (r_n,θ_n,ϕ_n) is the position of the nth Lagrangian marker. The dot represents differentiation with respect to the dimensionless time $\tau=10^{-3}t(g_s/R_\odot)^{1/2}$, where g_s is the surface gravity, $R_\odot$ the radius of the Sun and $\omega=10^3\Omega/(g_sR_\odot)^{1/2}=4.4$ for the solar values. M_n is the magnetic buoyancy of the nth point which is discussed in detail in Paper I. The thermal conditions we use to calculate magnetic buoyancy are as given in Eqs. (8) and (16) of

Paper I. The expressions for L_n, $c_n(k'_n)_\xi$, $c_n(k'_n)_\theta$ and $c_n(k'_n)_\phi$ are given in Paper I. D_ξ, D_θ and D_ϕ are the components of drag. The drag is modeled as the drag experienced by a cylinder moving in a fluid with its axis perpendicular to its direction of motion. The drag per unit length is

$$\boldsymbol{D}_n = -\tfrac{1}{2} C_D \rho_e(\xi_n) \sigma_n |\boldsymbol{v}_{k,n}| \boldsymbol{v}_{k,n}, \tag{8}$$

where C_D is a dimensionless constant which is roughly constant at large Reynolds numbers and has a value of 0.4 (Goldstein 1938), $\rho_e(\xi_n)$ is the density, σ_n the cross-sectional radius and $\boldsymbol{v}_{k,n}$ the velocity perpendicular to the local tangent at the nth point. We have $\boldsymbol{v}_{k,n} = \hat{\boldsymbol{l}} \times (\boldsymbol{v}_n \times \hat{\boldsymbol{l}})$, where $\boldsymbol{v}_n$ is the velocity and $\hat{\boldsymbol{l}}$ is the unit vector along the tangent at the nth point. The expression for $\hat{\boldsymbol{l}}$ was given in Paper I. The drag term as appearing in Eqs. (5)–(7) will be

$$\frac{\boldsymbol{D}_n}{\pi \sigma_n^2 \rho_e(\xi_n)} = -\frac{C_D}{2\pi\sigma_n} [v_n^2 - (\boldsymbol{v}\cdot\hat{\boldsymbol{l}})^2]^{1/2} [\boldsymbol{v}_n - (\boldsymbol{v}_n \cdot \hat{\boldsymbol{l}})\hat{\boldsymbol{l}}]. \tag{9}$$

Note that drag increases with decreasing flux tube size.

A full account of the specification of the initial state and the anchoring are given in Sects. 2.2 and 3 of Paper I. The initial configuration of the flux ring is taken to be lying on a θ-cone with a sinusoidal variation in ϕ and having the same temperature at every point as the surroundings. Reproducing Eq. (5) of Paper I, we take

$$\xi_0 = \xi_* + \xi_*^1 \sin m\phi, \tag{10}$$

where, ξ_* is 0.7, and ξ_*^1 is taken as the thickness of the overshoot region $= 0.015$ ($\sim 10^4$ km) and m is the number of loops per flux ring. Since we understand very little of the flux breakup process from the stable dynamo layer, it is difficult to ascertain what would be a truly realistic initial state. Our choice is merely one of convenience. Luckily, the final outcome seems not to depend much on the details of the initial state, as can be seen in the simulations of Moreno-Insertis (1986), Chou & Fisher (1989) and Choudhuri (1989), who arrive at similar situations starting from very different kinds of initial states.

Choudhuri (1990b) pointed out a small correction to Spruit's thin flux tube equations. The correction term is

$$\left[\frac{v_{c,n}^2}{2} - \frac{v_{c,n}}{k_n^2}\hat{\boldsymbol{l}}_n \cdot (\boldsymbol{\Omega} \times \hat{\boldsymbol{l}}_n)\right] \boldsymbol{k}_n,$$

where

$$v_{c,n} = -\frac{\hat{\boldsymbol{l}}_n}{k_n^2} \cdot \frac{\partial^2 \boldsymbol{v}_n}{\partial l_n^2}.$$

It has been seen that the inclusion of this term does not change the behaviour of the system qualitatively (Choudhuri 1990b). Including this term in a numerical code, however, poses some problems. Since this term has a second spatial derivative (which is higher than any other spatial derivative in the equation), it would be necessary to take a large number of points per loop to evaluate this term accurately. This increases the computational time enormously without adding anything of significance. Hence we have carried out our calculations without incorporating this term.

4. Calculating tilt

In this section, we illustrate the method of calculating the tilt of a flux loop by considering the example of a non-axisymmetric flux ring with an initial magnetic field of 100 kG starting from rest at a latitude of $\lambda = 30°$ at the bottom of the convection zone. The initial configuration of the non-axisymmetric flux ring is as given by Eq. (10) with $m = 4$.

The portions of the flux ring below the bottom of the convection zone are anchored by the subadiabatic gradient of the overshoot layer there as given in Eqs. (10) and (11) of Paper I. As seen in Paper I, in order to anchor fields smaller than 17 kG a subadiabatic gradient corresponding to a value of $\alpha = 10$ is sufficient (α was defined in Paper I as the magnitude of subadiabatic gradient in the overshoot layer divided by the superadiabatic gradient at the bottom of the convection zone). From Eq. (13) of Paper I, it follows that 100 kG fields starting with thermal equilibrium with the surroundings can be held anchored only by making the subadiabatic gradient sufficiently large with $\alpha \geq 10^3$ and 1000 kG fields can be anchored only if $\alpha \geq 10^5$. Here we choose a value of $\alpha = 10^3$. This is not because we have any reason to suspect such strong subadiabatic gradients, but rather because it merely provides us a way of anchoring these flux tubes. We still do not have any proper understanding of the anchoring problem. If, however, there is any mechanism for anchoring such strong magnetic fields, the behavior of the flux tube is not expected to be very different from what we get by achieving anchoring with an arbitrarily large subadiabatic gradient. It may be noted that Moreno-Insertis (1986) started with flux tubes in mechanical equilibrium and found that 100 kG flux tubes could be anchored even if they started from above the subadiabatic layer.

We see in Fig. 6c of Paper I that the anchored part of the flux tube slides towards higher latitudes when the Coriolis force is strong. In reality, however, if the dynamo region is packed with toroidal flux as shown in Fig. 21.1 of Parker (1979), then this sliding of the anchored flux tube would be inhibited by the magnetic flux in the nearby regions. One can mathematically stop the sliding by simply nullifying the θ velocity ($v_\theta = 0$) of the anchored regions at every iteration. This is done throughout the paper for all the calculations. The qualitative conclusions, however, do not change even if we had not stopped the latitudinal sliding.

The trajectory of the flux ring is obtained by integrating Eqs. (5)–(7) with $D = 0$, i.e. there is no drag on this flux ring. Figure 5a shows the positions of one flux loop of the flux ring in the ξ–ϕ plane at equal time intervals of 21.6 h.

The dark dots on each loop show the positions of the Lagrangian markers. The dashed line shows the final configuration of the loop when the top of the loop hits the top of the convection zone (i.e. touches $\xi = 1$). Figure 5b shows the loop in the θ–ϕ plane and the final configuration is marked by a dashed line. It is clear from the θ values that the flux tube has more or less emerged radially, as we expect in the case of a strong magnetic field of 100 kG. The final configuration (the dashed lines of Figs. 5a, b) of one loop of the flux ring is shown in Fig. 5c. The asymmetry in the ξ–ϕ plot shows the asymmetric mass downflow because of the Coriolis force as explained in Sect. 2. The asymmetry in the θ–ϕ plot is because of the tilt in the loop. If (θ_1, ϕ_1) and (θ_2, ϕ_2) are the positions of two sides of the loop at some ξ = constant sphere with ξ slightly smaller than 1, then the tilt can be taken to be

$$\gamma = \tan^{-1}\left[\frac{(\theta_2 - \theta_1)}{(\phi_2 - \phi_1)\sin\theta_{em}}\right], \tag{11}$$

where θ_{em} is the co-latitude at which the top of the loop touches $\xi = 1$. For the particular case under consideration, we have $\theta_{em} = 56.1°$, whereas (ϕ, θ) values at $\xi = 0.95$ are $(\phi_2 = 67°, \theta_2 = 59.6°)$ on the side of the p-spot, and $(\phi_1 = 26.4°, \theta_1 = 50°)$ on the side of the f-spot. For the values given above, γ turns out to be 15.9°. We choose the value $\xi = 0.95$ only for convenience. From Fig. 5c one can calculate the tilts that would be obtained if ξ is chosen to be any value other than $\xi = 0.95$. Figure 5d shows how the value of the tilt varies with ξ. The tilt has a maximum value of 17.1° at $\xi = 0.99$ and drops down almost linearly with ξ. So taking $\xi = 0.95$ would underestimate γ by about 1°. Figure 5d also shows how the tilts vary with ξ for some other combinations of magnetic field and latitude. For the rest of our calculations we shall calculate the tilts at

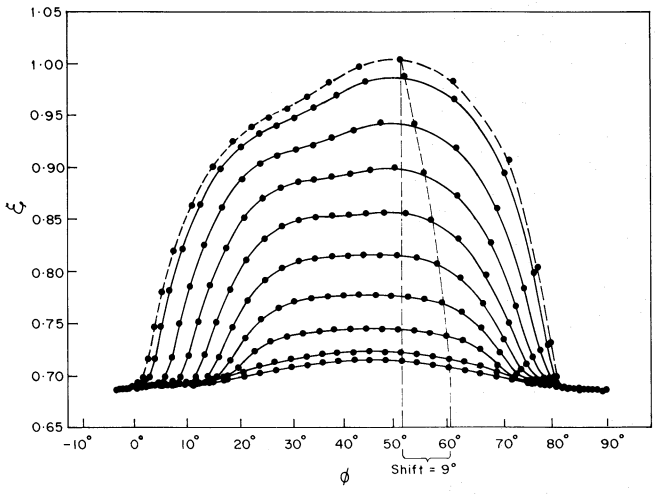

Fig. 5a. Evolution of a flux loop of 100 kG released at 30° latitude. The positions of the loop are in the ξ–ϕ plane at equal time intervals of 21.6 hours, except the final configuration (dashed line) which is 8.64 hours after the previous one

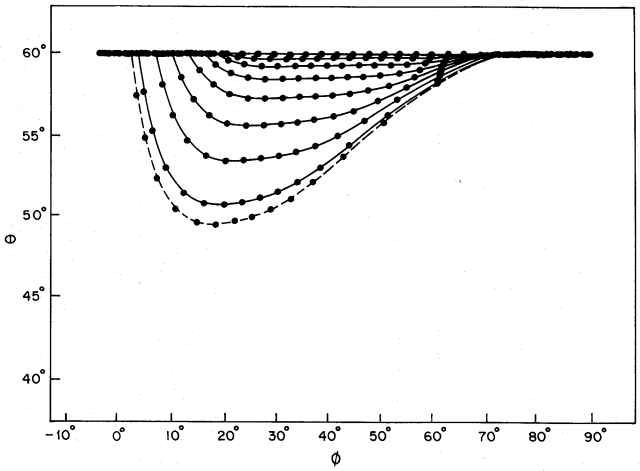

Fig. 5b. Same as Fig. 5a, except that the positions of the loop are in the θ–ϕ plane

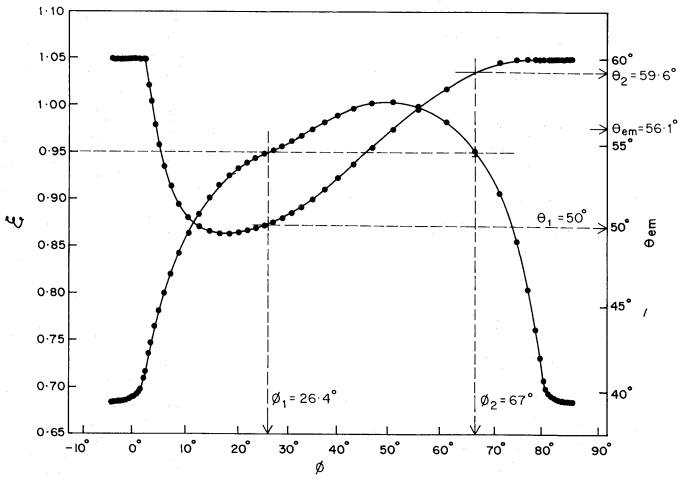

Fig. 5c. The final configurations in the ξ–ϕ plane as in Fig. 5a and in the θ–ϕ plane as in Fig. 5b

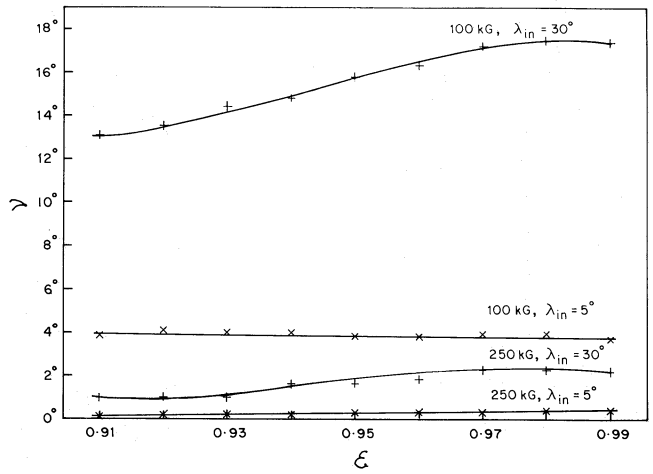

Fig. 5d. Plot of how tilt γ varies when it is calculated at different ξ, for flux loops of various field strengths released at various latitudes as indicated

$\xi = 0.95$. Choosing any other value of ξ between 0.90 and 0.99 will not have any drastic change on the results.

5. Results for no drag

We first present calculations without incorporating drag and with one loop in each quadrant, i.e. with $m = 4$. Flux loops with initial magnetic fields B_0 ranging from 10 to 1000 kG are released at 5° latitude at the bottom of the convection zone. For $B_0 < 250$ kG, α (which is a measure of the subadiabatic gradient in the overshoot layer) is taken to be 1000 and for $B_0 > 250$ kG, α is chosen as 10^5. The trajectories of the flux rings are computed by integrating Eqs. (5)–(7) with $D = 0$ and the final configurations of the rings are obtained. The tilt γ and emerging co-latitude θ_{em} of these flux loops are measured as described in Sect. 4 and plotted in Fig. 6a as a function of B_0.

(a) Flux loops with $B_0 > 60$ kG emerge radially at 5° latitude. This conforms with the results of an axisymmetric flux ring given in Choudhuri & Gilman (1987) and the non-axisymmetric rings of Choudhuri (1990). The rough calculations of Sect. 2 apply very well for these radially emerging flux loops. As shown in Fig. 6a the tilt increases as B_0 decreases according to Eq. (4) because the rise time increases with decreasing field strength. (b) For $B_0 < 60$ kG Coriolis force begins dominating over magnetic buoyancy and the top of the flux loops begin emerging at higher and higher latitudes. The tilt curve shows a rapid rise from 60 to 25 kG because they have a larger rise time. (c) For $B_0 < 25$ kG Coriolis force completely overcomes magnetic buoyancy and the top of the flux loops move parallel to the rotation axis.

The tilt and θ_{em} curves for flux loops released from 30° latitude are also shown in Fig. 6a. (a) Flux loops with $B_0 > 60$ kG emerge radially and their tilt curve lies above the 5° tilt curve because of the cos θ-effect which applies to all radially emerging flux loops. (b) Flux loops with 10 kG $< B_0 < 60$ kG do not emerge radially but at higher latitudes than the latitude at which they were released. They show larger tilts when released at 5° latitude than at 30° latitude. The cos θ-effect is no longer obeyed by these flux loops and they disobey Joy's Law. (c) Flux loops with $B_0 < 15$ kG show negative tilts and disobey Joy's law.

Flux loops of a given B_0 are released at 5°, 10°, 15°, 20°, 25°, 30° and 35° latitude at the bottom of the convection zone. The final configurations of the flux loops are obtained and the tilt angles are calculated as described in Sect. 4. Figure 6b plots sin γ against sin λ_{em} (λ_{em} is the latitude at which the top of the flux loop emerges) for different magnetic fields as indicated. The observational results are also shown in Fig. 6b [Wang & Sheeley 1991; Eq. (1)]. (a) Flux tubes with 100 kG magnetic field seem to fit the observations closely. Given the nature of various uncertainties in our model, results which differ from observations by factors not larger than two should be regarded as good fits. In that spirit, magnetic fields lying in the range 60 kG $< B_0 <$ 160 kG can be taken to be consistent with Joy's law. (b) Flux tubes with $B_0 > 160$ kG have the right kind of tilt and right kind of variation of tilt with latitude, but the values of the tilts are much smaller than the observed values. (c) Flux tubes with $B_0 < 60$ kG either show negative tilts or show tilts which decrease with increasing latitude which is against Joy's law. Fields smaller than 60 kG move parallel to the rotation axis and always emerge at high latitudes, hence the sin γ–sin λ_{em} curves for such fields lie in the region of high values of sin λ_{em}.

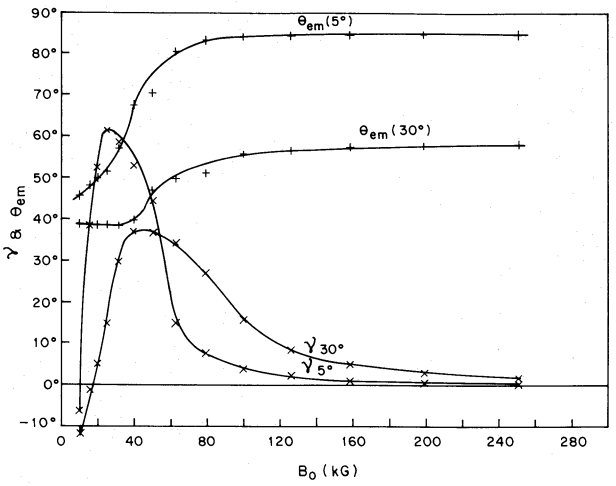

Fig. 6a. The plots of the tilts γ and emerging co-latitude θ_{em} of flux loops released at 5° and 30° latitude (as indicated) for different fields. There is no drag on the flux loops

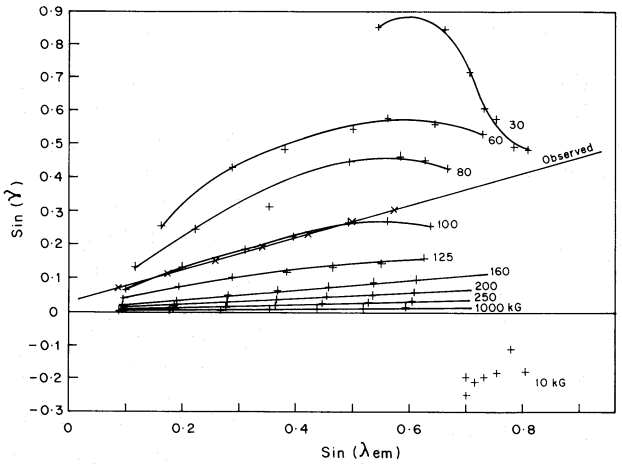

Fig. 6b. The plots of sin γ for flux loops released at various latitudes against sin λ_{em} for the fields indicated. There is no drag on the flux loops

Henceforth we will use the expressions "obey the weak form of Joy's law", "obey the strong form of Joy's law" and "disobey Joy's law". Flux loops are said to obey the weak form of Joy's law, when they show the right kind of tilt

with the p-limb towards the equator and the f-limb away from the equator and show the right kind of variation of tilt with latitude (i.e. the tilts increase with increasing latitude), but the values of tilt need not match the observations. The strong form of Joy's law is said to be obeyed when we find not only the right kind of tilt and the right kind of latitudinal variation of tilt, but the values of the tilt also are very close to the observed values. If they are said to disobey Joy's law then they either show negative tilts with the p-limb away from the equator or the tilts decrease with increase in latitude, which is against Joy's law.

Figures 6a, b suggest that the flux loops with $B_0 > 160$ kG emerge radially and obey only "the weak form of Joy's law", hence the possibility of their existence at the bottom of the convection zone may have to be ruled out. Fields < 60 kG automatically get ruled out because they disobey Joy's law. In the next two sections we show that this suggestion holds even when we include the drag and vary the footpoint separation. We shall see that these limits on the magnetic field fluctuate a bit, but not drastically.

6. Results with drag

Drag is incorporated by substituting Eq. (9) in Eqs. (5)–(7). Introducing drag has two opposing effects on the tilts of these flux loops, (i) it increases the tilt of a flux loop by increasing its rise time, provided the rise time is smaller than the rotational time of the Sun (if the rise time is larger than the rotational time, then the tilt decreases), (ii) it opposes the tilting motion of the flux loop because of the drag in the θ direction and hence decreases the tilt in general. In addition to these two effects, the drag acting on the limbs of the flux loops reduces its ϕ motion. This reduces the Coriolis force acting on the ϕ velocity. So flux loops of small fields for which Coriolis force overpowers magnetic buoyancy and makes them emerge at very high latitudes can be made to emerge radially by increasing drag. Drag can be increased by decreasing the flux tube radius [Eq. (9)]. When the flux tube radius is decreased to 10 km, all flux loops down to 10 kG emerge radially.

Since our understanding of the physical processes which produce flux tubes in the convection zone is still quite primitive, it is very difficult to make any estimate of the possible sizes of the flux tubes (Choudhuri 1992). One can, however, use the fact that the fibril flux tubes in the photosphere have fluxes of about 10^{19} Mx and demand that any flux tube should carry at least that much flux, though it is not clear at present whether the fibril flux tubes constitute merely an observational limit or a real physical limit. If we still use this limit on flux as a rough guide, we can get a limit on the minimum cross-sectional radius that a flux tube could have at the base of the convection zone, which is

$$\sigma_0 > \frac{1.7\,10^4}{\sqrt{B_0}}\ \text{km}, \qquad (12)$$

where B_0 is the initial magnetic field of the flux tube in gauss. This implies that a 10 kG flux tube should not have a radius less than about 170 km. In order to understand the mathematical properties of the problem, we would, however, present some calculations done for cross-sectional radii not satisfying the condition (12).

The fact that increasing drag may help suppressing the Coriolis force becomes clear from Fig. 7a, which shows the trajectories of the tops of 30 kG flux loops with different cross-sectional radii starting from 5° latitude. For $\sigma_0 =$ 10 000 km, the drag is very small and the Coriolis force is overpowering. By the time we go to a radius of 10 km, the drag becomes so large that the Coriolis force is completely

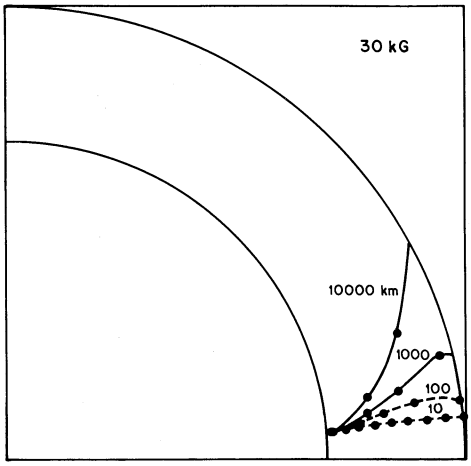

Fig. 7a. The trajectories in the ξ–θ plane of the topmost point of 30 kG flux loops released at 5° latitude for different initial cross-sectional radii σ_0 as indicated. The dark dots are at equal time intervals of 36 d

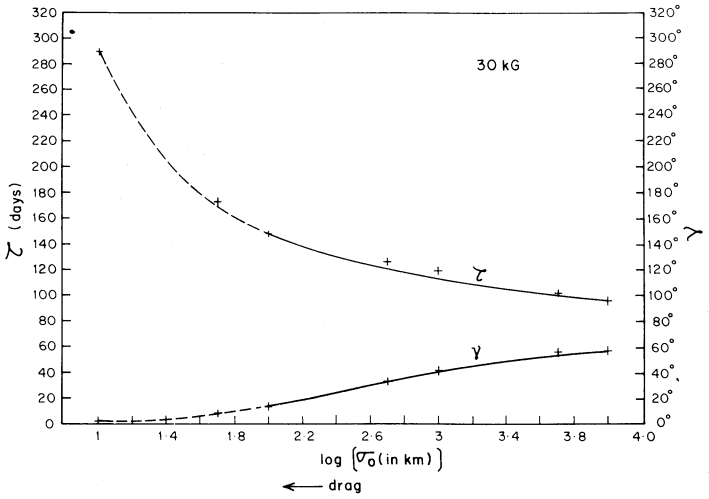

Fig. 7b. Plots of rise times τ and tilt angles γ of a 30 kG flux loop released at 5° latitude as a function of initial cross-sectional radius σ_0

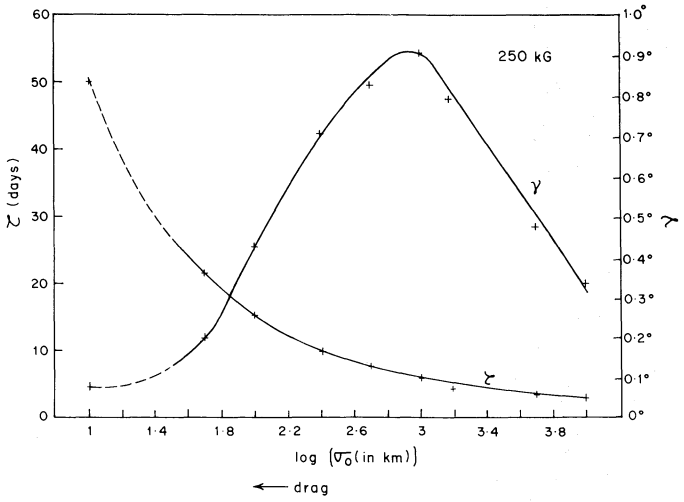

Fig. 7c. Plots of rise times τ and tilt angles γ of a 250 kG flux loop released at 5° as a function of cross-sectional radius σ_0

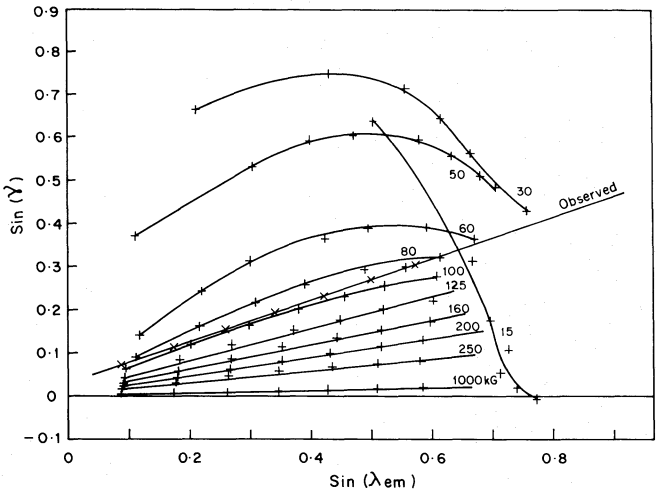

Fig. 8. The plots of sin γ for flux loops with $\sigma_0 = 1000$ km released at various latitudes against sin λ_{em} for the fields indicated

inhibited and the flux loop more or less emerges radially The trajectories for 100 km and 10 km are shown in dashed lines to indicate that the condition (12) is not satisfied in these cases so that they are of purely mathematical interest. The dots on the lines are at time intervals of 36 d. Clearly, the rise time increases with decreasing σ_0. Figure 7b shows the plot of the rise times and tilts with increasing σ_0. The rise times increase with increasing drag (decreasing σ_0). Since the rise time is always greater than the rotational time of the Sun, the additional increase in rise time due to drag results in a decrease in tilt as shown in Fig. 7b. The plots use dashed lines for the regions where the condition (12) is not satisfied. The decrease in tilt with increasing drag is contrary to what we expect from Eq. (4). Only if the rise time were less than the Sun's rotation period, then increasing drag would have made the rise time closer to the rotation period and tilt would increase with drag. This is seen in Fig. 7c, which shows rise times and tilts for a 250 kG flux tube starting from 5° latitude. The tilt is maximum when the rise time is about 10 d which is of the same order as the solar rotation period.

We now show how Fig. 6b get modified on the inclusion of drag. Figure 8 shows plots of the same quantities as shown in Fig. 6b, the only difference being that the calculations now included a drag term arising out of a finite cross-sectional radius $\sigma_0 = 1000$ km. There are no qualitative changes due to drag. Figure 9 presents results for $\sigma_0 = 100$ km when the drag becomes much stronger and some changes are noticeable. The plot for 25 kG in Fig 9 uses a dashed line to indicate that the condition (12) is not satisfied. The general observation is that the tilts are smaller in Fig. 9 compared to Figs. 6b and 8. Previously 60 kG was taken as a lower limit of magnetic field for which the strong form of Joy's law was obeyed. Now it appears that fields somewhat weaker (though not much weaker) than 60 kG also may obey Joy's law to some

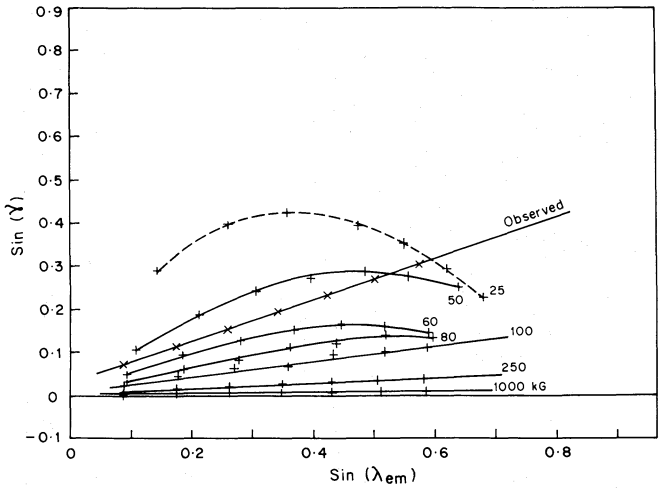

Fig. 9. The plots of sin γ for flux loops with $\sigma_0 = 100$ km released at various latitudes against sin λ_{em} for the fields indicated

extent, though there is a tendency of the curves becoming convex instead of being straight lines in accordance with Joy's law. Thus our conclusions in the previous section remain valid even after the inclusion of drag.

7. Effect of magnetic tension

All the above calculations were done for flux rings with $m = 4$, which at 5° latitude is equivalant to a footpoint separation of $0.7\pi R_\odot \cos \lambda_{in}/m = 3.81\,10^5$ km. If the footpoint separation is decreased, tension plays an important role in the evolution of these flux loops. Magnetic tension has three important effects on the rising flux loops: (i) A component of tension acts in the direction opposite to magnetic buoyancy and hence increases the rise time.

Increase in rise time increases or decreases the tilt of the flux loops depending on whether the rise time approaches the rotational time of the Sun or increases beyond it. (ii) Tension in general opposes any deformation in the flux tube and hence it opposes the tilting of the flux loop too. This effect reduces the tilt of the flux loop. (iii) A very large tension can prevent the rising portion of the flux loop from moving in the ϕ direction because motion in the ϕ direction amounts to deformation of the flux loop. Recalling that the Coriolis force acting on the ϕ motion of the rising portions of the flux tubes is responsible for the tops of the flux loops to appear at very high latitudes, any inhibition of the ϕ motion makes the tops of the flux loops appear at low latitudes. When tension is increased by reducing the footpoint separation, the flux loops begin emerging at lower and lower latitudes.

We first consider how the trajectories of the flux tubes are modified on changing the footpoint separation. A 30 kG flux loop is released at 5° latitude at the bottom of the convection zone. The initial configuration of the loop is taken to be given by Eq. (10) with the following values of $m=4, 8, 12$. The trajectories of the flux loops are obtained by integrating Eqs. (5)–(7) with zero drag. The lines marked 4 and 8 in Fig. 10a show the trajectories of the top of the flux loop in the θ–ξ plane for the $m=4$ and $m=8$ cases. Though the Coriolis force is strong, the $m=8$ loop emerges at a somewhat lower latitude compared to the $m=4$ loop. It is also to be noted that the $m=8$ flux loop takes an enormously long time to rise (about 8 yr), since its rise is almost halted at a point of its trajectory due to the strong magnetic tension. When the magnetic tension is increased further by taking $m=12$, the outward motion of the flux tube is completely stopped after a small rise. A similar result was found by Chou & Fisher (1989). Figure 10b shows the rise times and tilts for different footpoint separations (i.e. for different values of m) for the 30 kG flux tubes we are considering. Though m is not a continuous variable, we have joined the discrete points in the plot through smooth curves. It is clear that the rise time increases with decreasing footpoint separation. Since the rise time for $m=4$ is already larger than the rotational time of the Sun, any further increase in rise time due to decrease in footpoint separation is expected to decrease the tilt angle. The tilt curve in Fig. 10b shows exactly that.

In situations where the rise time is less than the solar rotation period, the tilt may increase when the rise time is increased due to decreasing footpoint separation. This is seen in Fig. 10c, which shows the rise times and tilts for a 250 kG flux loop with different footpoint separations. The tilt is maximum when the rise time is about three days,

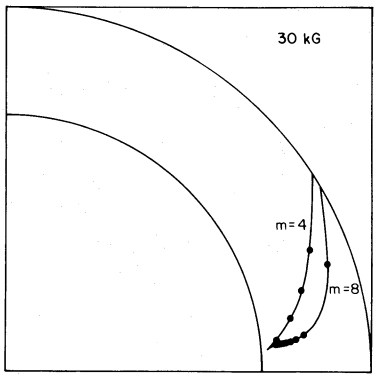

Fig. 10a. The trajectories in the ξ–θ plane of the topmost point of 30 kG flux loops released at 5° latitude for different footpoint separations corresponding to $m=4$ and $m=8$. For $m=4$ loop the dark dots are at time intervals of 18 d and for $m=8$ loop they are at time intervals of roughly 1 yr

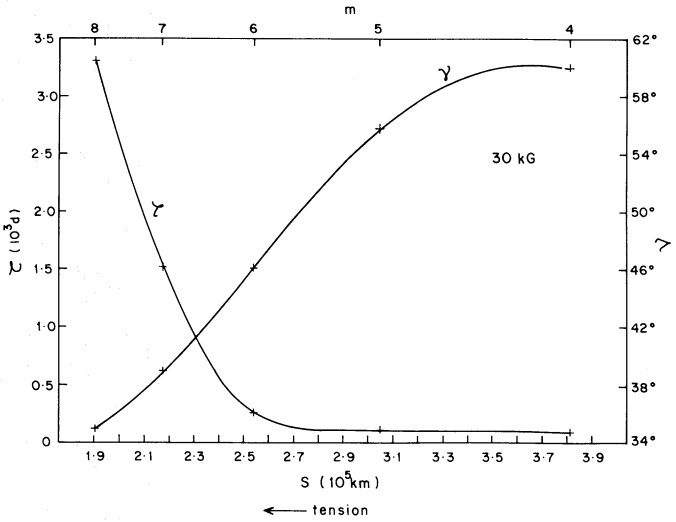

Fig. 10b. Plots of rise times τ and tilt angles γ of a 30 kG flux loop released at 5° as a function of footpoint separations s

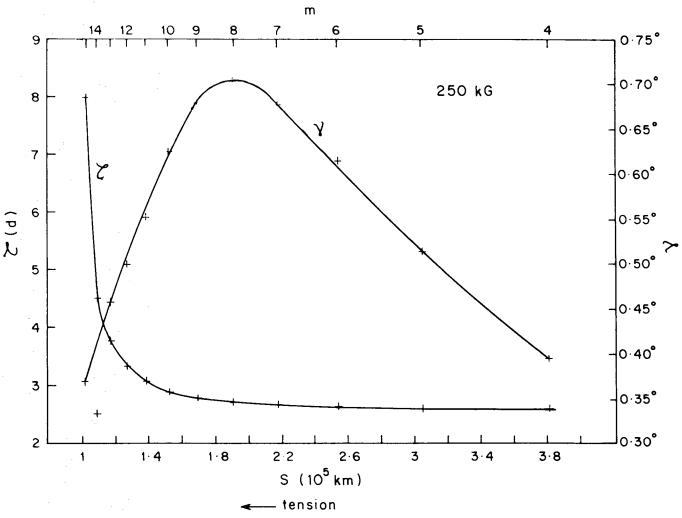

Fig. 10c. Plot of rise times τ and tilt angles γ of a 250 kG flux loop released at 5° as a function of footpoint separations s

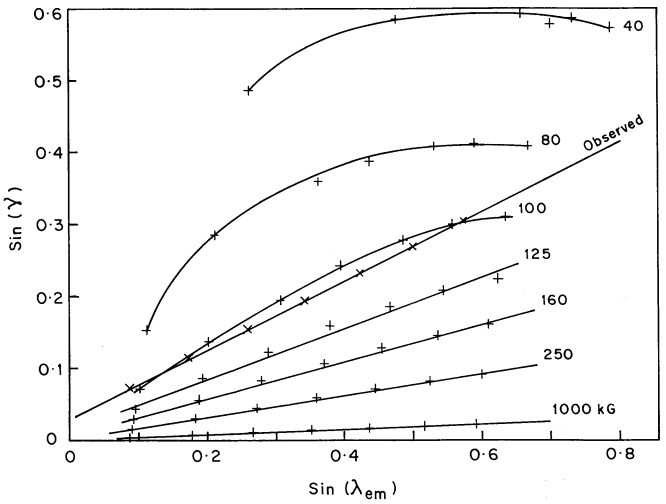

Fig. 11. The plots of sin γ for flux loops with footpoint separation $s = 1.91\ 10^5$ km ($m = 8$) released at various latitudes against sin λ_{em} for the fields indicated. There is no drag on the flux loops

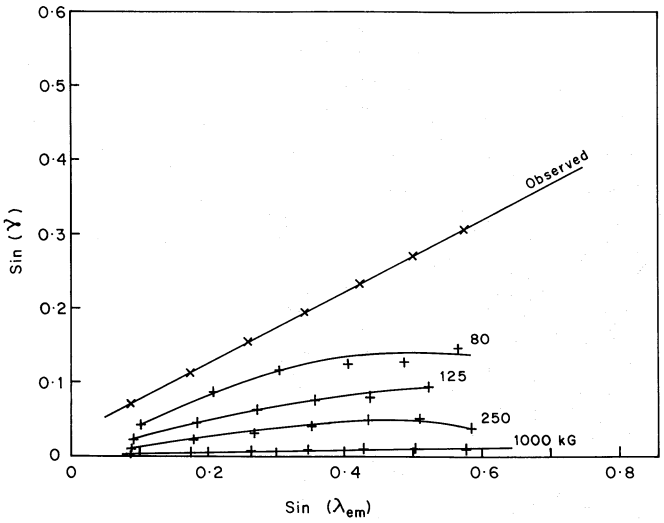

Fig. 12. The plots of sin γ for flux loops with footpoint separation $s = 1.27\ 10^5$ km ($m = 12$) released at various latitudes against sin λ_{em} for the fields indicated. There is no drag on the flux loops

which is within one order of magnitude of the solar rotation period.

We repeat the calculations of Sect. 5 by reducing the footpoint separation by changing the value of m from 4 to 8. Figure 11 shows the sin γ–sin λ_{em} curves. The computations were stopped at 30 kG because flux tubes with weaker fields do not emerge to the surface, as their rise is halted by magnetic tension. (a) Fields above 160 kG obey only the weak form of Joy's law. (b) Fields between 40 and 160 kG obey the strong form of Joy's law. (c) Fields between 40 and 25 kG disobey Joy's law. (d) Fields below 25 kG attain an equilibrium configuration inside the convection zone and do not emerge.

The footpoint separation is further reduced by increasing m to 12. Figure 12 shows the sin γ–sin λ_{em} curves. Fields below 80 kG attain an equilibrium separation well within the convection zone and cannot emerge to the surface. When compared to Fig. 11, the tilts are considerably smaller for the corresponding field strengths. Only the weak form of Joy's law holds for fields above 125 kG, and it is not possible to match the observations for any value of the magnetic field.

For $m = 16$ even megagauss fields fail to emerge from the convection zone. Figure 13 gives the critical footpoint separation for different magnetic fields below which the flux loops cannot emerge from the convection zone. The flux tube stops rising when the magnetic tension overcomes the magnetic buoyancy. Since both magnetic tension and magnetic buoyancy go as the square of the magnetic field, one may expect that the critical footpoint separation would be independent of the magnetic field. In fact, the critical footpoint separation for the strong fields has a constant value $0.98\ 10^5$ km which is comparable to the scale height at the base of the convection zone. Parker (1979, p. 338) looked at an analytical model which became

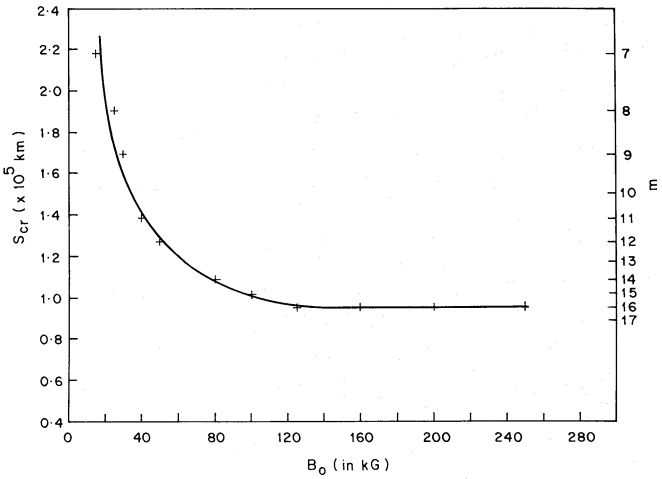

Fig. 13. Plot of the critical footpoint separations s_{cr} with initial magnetic fields B_0. Flux loops in the parameter regime below this curve cannot emerge from the convection zone

unstable for footpoint separations larger than 2π times the scale height. Chou & Fisher (1989) found that the critical footpoint separation for their model was $1.97\ 10^5$ km, which is about twice our value. Thus the results for different models are in qualitative agreement. When the magnetic field is weaker, however, the Coriolis force also starts playing a role in suppressing magnetic buoyancy and the rise of flux tubes can be stopped with weaker magnetic tension (i.e. larger footpoint separation).

To summarize, the flux loop can rise to the solar surface only if the footpoint separation is not less than a critical value. For flux loops which are able to come to the surface, the conclusions of the last sections more or less hold. We have not studied $m < 4$ cases in detail, since the

typical separations of bipolar sunspots seem to suggest that m in the range 4–12 is about right. Probably this is because of the fact that the flux strands which break out of the stable layer have limited extents in the longitudinal direction.

8. Conclusions

We have seen that the tilts of bipolar magnetic regions can be explained most naturally as resulting from the action of the Coriolis force on the flux loops rising from the base of the convection zone. If no special mechanism is invoked to inhibit the ϕ-motion and thereby reduce the Coriolis force, then flux loops with magnetic fields in the range 60–160 kG come out with the correct amount of tilt, provided the footpoint separation of the loop is not small enough for magnetic tension to stop its rise. For magnetic fields lying in this range, the rise time is comparable to the solar rotation period. Another way of putting the same thing is that the magnetic buoyancy for these fields is comparable to the Coriolis force and is just capable of making the flux loops rise radially. If magnetic buoyancy is much stronger, then the flux loops come out with negligible tilt. On the other hand, if magnetic buoyancy were weaker, then the flux will move parallel to the rotation axis and emerge at wrong latitudes.

These conclusions pose the question whether there is any deep reason for the various quantities to have values which make the magnetic buoyancy only marginally stronger than the Coriolis force. We are unable to offer any explanation for such a remarkable coincidence. There are many other questions which are equally baffling. Since the magnetic energy density for such strong fields will be orders of magnitude larger than the kinetic energy density of convective turbulence, we fail to understand how the dynamo may operate in a region with such strong fields or how such fields may even come into being. One may of course suggest that the dynamo first produces weaker fields which are strengthened by some mysterious mechanism not yet known to us. Then there is the question of storing such strong fields in a stable layer so that parts of the flux tubes can remain anchored. In our calculations, we have achieved the anchoring by making the subadiabatic gradient in the overshoot layer arbitrarily large, which is a purely mathematical device without the slightest physical sanction. The storage problem has recently been studied by Moreno-Insertis et al. (1992) who suggest that it may be possible to store fields up to about 100 kG or so in the overshoot layer. A strong field, however, would solve a difficulty pointed out by Parker (1987). He argued that an equipartition field packed in the thin overshoot layer would be insufficient to produce the flux that we see in the active regions. With a stronger field, this problem disappears.

These difficulties with the strong fields perhaps suggest that we should take a closer look at weak fields. In the paper under preparation (D'Silva 1993), we shall show that, if we invoke mechanisms for suppressing ϕ-motions so that weak fields may come out radially with appropriate tilts, then so many possibilities open up that it is impossible to say anything definitively. The really strong conclusion that can be made in the present paper is that the magnetic fields of the rising flux tubes could not be much larger than 160 kG. Otherwise the tilts of the bipolar magnetic regions would have been miniscule.

Acknowledgements. We wish to thank the referee of this paper, Dr. Manfred Schüssler, whose valuable comments helped us improve the manuscript. Sydney D'Silva was supported by a research fellowship from the Council of Scientific and Industrial Research (C.S.I.R), India.

Appendix: Differential rotation

In order to show that the amount of differential rotation present in the Sun is not sufficient to influence the dynamics of flux tubes, we consider the motion of an axisymmetric flux ring incorporating the differential rotation. Helioseismology observations (Dziembowski et al. 1989) show that the contours of constant Ω lie on cones. The surface differential rotation varies roughly from $\Omega_{eq} = 1/25\ d^{-1}$ at the equator to $\Omega_{pole} = 1/30\ d^{-1}$ at the poles. We can take $\Omega(r, \theta)$ inside the convection zone in the form

$$\Omega(r, \theta) = \Omega_{eq}(1 - A \cos\theta), \quad (0.7 \leq r \leq 1),$$

with $A = 5/30$.

The equation of motion for a flux ring in the presence of differential rotation is given in (B2)–(B4) in Appendix B of Choudhuri & Gilman (1987). We study the dynamics with the drag equal to zero. In Eq. (B4), which becomes

$$\frac{d}{dt}\left\{r^2\left[\Omega(r, \theta) + \left(\frac{d\phi}{dt}\right)\right]\sin^2\theta\right\} = 0,$$

it is to be noted that $\Omega(r, \theta)$ cannot be taken outside the time derivative as a constant, even though the differential rotation does not change with time. This is because of the fact that the Lagrangian time derivative of Ω is

$$\frac{d\Omega}{dt} = \frac{\partial\Omega}{\partial t} + \boldsymbol{v} \cdot \nabla\Omega,$$

which in the present context becomes

$$\frac{d\Omega}{dt} = A\Omega_{eq}\dot{\theta}\sin\theta.$$

The dotted line in Fig. 14 is a contour for constant angular momentum with $A = 0.5$. Note that the departure of the constant angular momentum contour from the solid body rotation one is marginal, despite A being as large as 0.5. For $A = 5/30$, the contour is almost parallel to the rotation axis. The constant angular momentum contour is almost

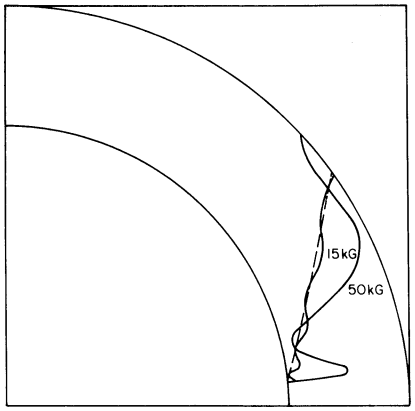

Fig. 14. Trajectories of a 15 and 50 kG axisymmetric ($m=0$) flux loop in the $\xi-\theta$ plane, released at 5° latitude at the bottom of the convection zone. The dashed line shows the contour of constant angular momentum

parallel to the rotation axis even if we use the differential rotation profile of Howard & Harvey (1970) with the assumption that Ω is constant along cones.

A 10 kG axisymmetric flux ring is released at 5° at the bottom of the convection zone in this differentially rotating convection zone with $A=0.5$. Figure 14 shows the trajectory of this flux ring in the $\xi-\theta$ plane. The flux ring hugs the contour of constant angular momentum which is almost parallel to the rotation axis. A 50 kG flux ring released at 5° also oscillates about this contour and emerges at a high latitude. If we take the solar value of $A=5/30$, the trajectories are almost indistiguishable from the trajectories in the solid body rotation case. Since the introduction of a differential rotation shows only a marginal difference in the dynamics of the flux tubes, we use solid body rotation in all our calculations in order to understand the physics better.

References

Babcock H.W., 1961, ApJ 133, 572
Chou D.Y. Fisher G.H., 1989, ApJ 341, 533
Choudhuri A.R., 1989, Sol. Phys. 123, 217 (Paper I)
Choudhuri A.R., 1990a, ApJ 355, 733
Choudhuri A.R., 1990b, A&A 239, 335
Choudhuri A.R., 1992, in: Thomas J.H., Weiss N.O. (eds.) Sunspots-Theory and Observations. Nato ARW, Kluwer, Dordrecht, p. 243
Choudhuri A.R., D'Silva S., 1990, A&A 239, 326
Choudhuri A.R., Gilman P.A., 1987, ApJ 316, 788
D'Silva S., 1993, ApJ (in press)
D'Silva S., Choudhuri A.R., 1991, Sol. Phys. 136, 201
Dziembowski W.A., Goode P.R., 1989, ApJ 347, 540
Dziembowski W.A., Goode P.R., Libbrecht K.G., 1989, ApJ 337, L53
Goldstein S., 1938, Modern Developments in Fluid Mechanics. Clarendon Press, Oxford, p. 418
Hale G.E., Ellerman F., Nicholson S.B., Joy A.H., 1919, ApJ 49, 153
Howard R.F., 1992, Sol. Phys. 137, 205
Howard R.F., Harvey J., 1970, Sol. Phys. 12, 23
Leighton R.B., 1964, ApJ 140, 1547
Leighton R.B., 1969, ApJ 156, 1
Moreno-Insertis F., 1986, A&A 166, 291
Moreno-Insertis F., Schüssler M., Feriz-Mas A., 1992, A&A (submitted)
Parker E.N., 1955, ApJ 122, 293
Parker E.N., 1975, ApJ 198, 205
Parker E.N., 1979, Cosmical Magnetic Fields. Clarendon Press, Oxford
Parker E.N., 1987, ApJ 312, 868
Schmidt H.U., 1968, in Kiepenheuer K.O. (ed.) Structure and Development of Solar Active Regions. Proc. IAU Symp. 35, 95
Shibata K., Tajima T., Steinolfson R.S., Matsumoto R., 1989, ApJ 345, 548
Shibata K., Nozawa R., Matsumoto R., Sterling A.C. Tajima T., 1990, ApJ 351, L25
Spruit H.C., 1981, A&A 98, 155
Wang Y.M., Sheeley N.R., 1989, Sol. Phys. 124, 81
Wang Y.M., Sheeley N.R., 1991, ApJ 375, 761